
Particle-based Energetic Variational Inference

Yiwei Wang^{* 1} Jiu hai Chen^{* 1} Lulu Kang¹ Chun Liu¹

Abstract

We introduce a new variational inference framework, called energetic variational inference (EVI). The novelty of the EVI lies in the new mechanism of minimizing the KL-divergence, or other variational object functions, which is based on the energy-dissipation law. Under the EVI framework, we can derive many existing particle-based variational inference (ParVI) methods, such as the classic Stein variational gradient descent (SVGD), as special schemes of the EVI with particle approximation to the probability density. More importantly, many new variational inference schemes can be developed under this framework. In this paper, we propose one such particle-based EVI scheme, which performs the particle-based approximation of the density first and then uses the approximated density in the variational procedure. Thanks to this Approximation-then-Variation order, the new scheme can maintain the variational structure at the particle level, which enables us to design an algorithm that can significantly decrease the KL-divergence in every iteration. Numerical experiments show the proposed method outperforms some existing ParVI methods in terms of fidelity to the target distribution.

1. Introduction

Bayesian methods play an important role in statistics and modern data analysis. They provide a rigorous framework for uncertainty quantification of various statistical learning models (Stuart, 2010; Gelman et al., 2013). The key step in Bayesian inference is to compute the posterior distribution $\rho(\mathbf{x}|\{\mathbf{y}_i\}_{i=1}^I)$ of certain unknown parameters $\mathbf{x} \in \mathbb{R}^d$. The main components of a Bayesian model includes, a set of data points $\{\mathbf{y}_i\}_{i=1}^I$ and each $\mathbf{y}_i \in \mathbb{R}^D$, the model assumption of the likelihood of the data $\rho(\{\mathbf{y}_i\}_{i=1}^I|\mathbf{x})$, and a user-specified prior distribution $\rho_0(\mathbf{x})$. Following the Bayes' theorem, the posterior distribution of the unknown

parameters is

$$\rho(\mathbf{x}|\{\mathbf{y}_i\}_{i=1}^I) = \frac{\rho(\{\mathbf{y}_i\}_{i=1}^I|\mathbf{x})\rho_0(\mathbf{x})}{\rho(\{\mathbf{y}_i\}_{i=1}^I)}.$$

It is a well-known challenge to compute the posterior distribution in practice. Many complex Bayesian models require approximate inference methods to compute the posterior.

Two classes of methods have been developed to approximate the posterior distribution: Markov Chain Monte Carlo (MCMC) sampling methods (Metropolis et al., 1953; Hastings, 1970; Geman & Geman, 1984; Welling & Teh, 2011) and variational inference methods (Jordan et al., 1999; Neal & Hinton, 1998; Wainwright et al., 2008; Blei et al., 2017). MCMC is a family of methods that draw samples from the target distribution through a Markov chain. Examples include random walk Metropolis (Metropolis et al., 1953), Gibbs sampling (Geman & Geman, 1984) and Stochastic gradient Markov chain Monte Carlo (Welling & Teh, 2011), etc. The Variational Inference (VI) framework essentially transforms the inference problem into an optimization problem, which minimizes some kind of distance functional over a prescribed family of distributions \mathcal{Q} (Blei et al., 2017). The distance functional measures the difference between a distribution and the target distribution. For Bayesian models, the target distribution is the posterior distribution. VI has a wide application that goes beyond Bayesian statistics and is a powerful tool to approximate probability densities. A common choice of the distance functional is the Kullback-Leibler (KL) divergence. For any two distributions $\rho(\mathbf{x})$ and $\rho^*(\mathbf{x})$, the KL-divergence is given by

$$\text{KL}(\rho(\mathbf{x})||\rho^*(\mathbf{x})) = \int \rho(\mathbf{x}) \ln \left(\frac{\rho(\mathbf{x})}{\rho^*(\mathbf{x})} \right) d\mathbf{x}. \quad (1.1)$$

The VI framework minimizes $\text{KL}(\rho(\mathbf{x})||\rho^*(\mathbf{x}))$ with respect to $\rho \in \mathcal{Q}$ in order to approximate the target distribution ρ^* . In traditional VI methods (Blei et al., 2017), \mathcal{Q} is often taken as a family of parametric distribution. Recently, there have been growing interests in flow-based VI methods, in which \mathcal{Q} consists of distributions obtained by a series of smooth transforms from a tractable initial reference distribution. Examples include normalizing flow VI methods (Rezende & Mohamed, 2015; Kingma et al.,

¹Department of Applied Mathematics, Illinois Institute of Technology, Chicago, USA. Correspondence to: Yiwei Wang <ywang487@iit.edu>. ^{*}Equal contribution.

2016; Salman et al., 2018) and particle-based VI methods (ParVIs) (Liu & Wang, 2016; Liu, 2017; Liu & Zhu, 2018; Chen et al., 2018; Liu et al., 2019; Chen et al., 2019). One ParVI method that has attracted much attention is Stein Variational Gradient Descent (SVGD) (Liu & Wang, 2016; Detommaso et al., 2018; Wang et al., 2019; Li et al., 2019). In fact, many existing ParVI methods can be viewed as some version of the approximated gradient flow of the KL-divergence (Liu, 2017). But these methods may not preserve the gradient flow structure at the particle level due to the fact that approximation of the density function is performed after the variational procedure, which is explained in Section 3.

Inspired by the *energy-dissipation law* of any dynamic system in physics, we propose a new mechanism to minimize the KL-divergence by employing an energetic variational approach, and thus we name it *Energetic Variational Inference (EVI)* framework. It is a very general framework. Using it, we can derive and explain many existing ParVI methods, such as the SVGD method. More importantly, many new ParVI schemes can be developed under the EVI framework. In this paper, we propose one such particle-based EVI scheme, which performs the particle-based approximation of the density first and then uses the approximated density in the variational procedure. Thanks to this "Approximation-then-Variation" order, we can derive a system of ordinary differential equations (ODEs) of particles that preserves the variational structure at the particle level, which is different from most of existing methods. By solving such an ODE system via the implicit Euler method, we can significantly decrease the discrete KL-divergence in every iteration and push the density of the particles close to the target distribution efficiently.

2. Energetic Variational Inference

2.1. Minimizing KL Divergence Through Flow Maps

The goal of the VI framework is to find a density function ρ from a family of density functions \mathcal{Q} , by minimizing the KL-divergence between $\rho(\mathbf{x})$ and the target density function $\rho^*(\mathbf{x})$. The complexity of this optimization problem is decided by the feasible region, i.e., the family \mathcal{Q} . In the flow-based VI methods, the set \mathcal{Q} consists of distributions obtained by smooth transforms of a tractable initial reference distribution (Li et al., 2019). In fact, the idea of using maps to transform a distribution to another has been explored in many earlier papers (Tabak et al., 2010; El Moselhy & Marzouk, 2012). Specifically, given a tractable reference distribution $\rho_0(\mathbf{z}) : \mathcal{X}_0 \rightarrow \mathbb{R}^+$ and a sufficient smooth one-to-one map $\phi(\cdot)$, such that $\mathbf{x} = \phi(\mathbf{z})$,

the family \mathcal{Q} is defined by

$$\mathcal{Q} = \{\rho | \rho_{[\phi]}(\mathbf{x}) = \rho_0(\phi^{-1}(\mathbf{x})) |\det(\nabla_{\mathbf{x}} \phi^{-1}(\mathbf{x}))|, \text{ where } \mathbf{x} = \phi(\mathbf{z}), \phi : \mathcal{X}_0 \rightarrow \mathcal{X} \text{ is a smooth one-to-one mapping.}\} \quad (2.1)$$

We assume $\mathcal{X}_0 = \mathcal{X} = \mathbb{R}^d$ through out this paper, but all the results can be directly applied to the $\mathcal{X}_0 \neq \mathcal{X}$ case. Moreover, we can enforce $\det(\nabla_{\mathbf{z}} \phi(\mathbf{z})) > 0$ since ϕ is one-to-one.

Given \mathcal{Q} in (2.1), solving the following problem

$$\rho_{\text{opt}} = \arg \min_{\rho \in \mathcal{Q}} \text{KL}(\rho || \rho^*) \quad (2.2)$$

is equivalent to finding the optimal smooth one-to-one map ϕ_{opt} such that

$$\rho_{\text{opt}}(\mathbf{x}) = \rho_0(\phi_{\text{opt}}^{-1}(\mathbf{x})) \det(\nabla_{\mathbf{x}} \phi_{\text{opt}}^{-1}(\mathbf{x})).$$

It usually requires a number of transformations, say K steps, to find the optimal map, or equivalently,

$$\phi_{\text{opt}}(\cdot) = \psi^K \circ \psi^{K-1} \dots \circ \psi^1(\cdot).$$

Each $\psi^t(\cdot)$ is a smooth and one-to-one map such that $\mathbf{x}^t = \psi^t(\mathbf{x}^{t-1})$. At the t th step, suppose $\phi^t(\cdot) = \psi^t \circ \psi^{t-1} \dots \circ \psi^1(\cdot)$ is a proper transform, then

$$\begin{aligned} \rho^t(\mathbf{x}^t) &= \rho^{t-1}((\psi^t)^{-1}(\mathbf{x}^t)) \det(\nabla(\psi^t)^{-1}(\mathbf{x}^t)) \\ &= \rho_0(\mathbf{x}^t) \det(\nabla(\phi^t)^{-1}(\mathbf{x}^t)). \end{aligned}$$

Apparently, the series of transformations need to move the initial density ρ_0 closer and closer to the target density ρ^* and eventually achieve convergence in terms of KL-divergence. Therefore, $\text{KL}(\rho^t || \rho^*)$ should be decreased after each step, i.e., $\text{KL}(\rho^t || \rho^*) - \text{KL}(\rho^{t-1} || \rho^*) \leq 0$.

If we generalize the meaning of t from the discrete step index to the continuous time $t \in [0, \infty)$, we can consider $\rho(\mathbf{x}, t) = \rho^t(\mathbf{x})$ as a density function evolving continuously with respect to time t , and such that $\frac{d}{dt} \text{KL}(\rho(\mathbf{x}, t) || \rho^*) \leq 0$. In the reminder of this section, we show how to use the energy-dissipating law to specify $\frac{d}{dt} \text{KL}(\rho(\mathbf{x}, t) || \rho^*)$, i.e., the speed of decreasing $\text{KL}(\rho(\mathbf{x}, t) || \rho^*)$.

2.2. Energetic Variational Inference

The goal is to find ϕ^t that minimizes the KL-divergence when $t \rightarrow \infty$. Since ϕ^t is a smooth one-to-one map, it can be defined through a smooth, bounded velocity field $\mathbf{u} \in \mathbb{R}^d \times [0, \infty)$ as in Definition 1. This definition is also used in (Sonoda & Murata, 2019). Here we exchange the two notation $\phi(\mathbf{z}, t) = \phi^t(\mathbf{z})$.

Definition 1. For a given smooth, bounded velocity field $\mathbf{u} \in \mathbb{R}^d \times [0, \infty)$, a flow map $\phi^t(\mathbf{z}) : \mathbb{R}^d \rightarrow \mathbb{R}^d$ is a map

given by an ordinary differential equation (for any fixed \mathbf{z})

$$\begin{cases} \frac{d\phi^t(\mathbf{z})}{dt} = \mathbf{u}(\phi^t(\mathbf{z})), & \mathbf{z} \in \mathbb{R}^d, \quad t > 0 \\ \phi^0(\mathbf{z}) = \mathbf{z}, & \mathbf{z} \in \mathbb{R}^d \end{cases} \quad (2.3)$$

Intuitively, \mathbf{u} is the speed of the probability mass, which is transported due to the transform ϕ^t . Due to this relationship (2.3), we can decide the transform ϕ^t by specifying \mathbf{u} . The idea of EVI is to specify \mathbf{u} through an energy-dissipation law.

In a physics system, an *energy-dissipation law*, given by

$$\frac{d}{dt}\mathcal{F}[\phi] = -2\mathcal{D}[\phi, \phi_t], \quad (2.4)$$

describes how the total energy of the system decreases with time, which is a consequence of the First and Second Law of thermodynamics. Here \mathcal{F} is the free energy, $-2\mathcal{D} \leq 0$ is the rate of energy dissipation, ϕ denotes system state, and ϕ_t is the derivative of ϕ with respect to t . One can view (2.4) as a generalization of gradient flow (Hohenberg & Halperin, 1977). As an analogy to physics, the KL-divergence serves as the *Helmholtz free energy* or *variational free energy* (Murphy, 2012), i.e., $\mathcal{F} = \text{KL}(\rho(\mathbf{x}, t) \parallel \rho^*)$. We can impose the energy-dissipation law as the mechanism that KL-divergence decreases with respect to time, or equivalently, let

$$\frac{d}{dt}\text{KL}(\rho(\mathbf{x}, t) \parallel \rho^*) = - \int \eta(\rho) |\mathbf{u}|^2 d\mathbf{x}, \quad (2.5)$$

where $\mathcal{D} = \frac{1}{2} \int \eta(\rho) |\mathbf{u}|^2 d\mathbf{x} > 0$ is the dissipation of the KL-divergence, and η is a user-specified positive functional of ρ . We use $|\mathbf{a}| = \sqrt{\mathbf{a}^\top \mathbf{a}}$, $\forall \mathbf{a} \in \mathbb{R}^d$ through this paper. Since $\rho(\mathbf{x}, t)$ is determined by $\phi(\mathbf{z}, t)$, $\rho(\mathbf{x}, t)$ can be considered as a functional of ϕ and denoted by $\rho_{[\phi]}$. Accordingly, the KL-divergence and the dissipation can be written as $\text{KL}(\rho_{[\phi]} \parallel \rho^*)$ and $\mathcal{D} = \frac{1}{2} \int \eta(\rho_{[\phi]}) |\phi_t|^2 d\mathbf{x}$, respectively.

Remark 2.1. *In the framework of energetic variational approach, a more complicated form of energy-dissipation law can be considered. For instance, we can take the energy-dissipation law as (Liu & Wang, 2020)*

$$\frac{d}{dt}\text{KL}(\rho(\mathbf{x}, t) \parallel \rho^*) = - \int \eta(\rho) |\mathbf{u}|^2 + \nu(\rho) |\nabla \mathbf{u}|^2 d\mathbf{x}, \quad (2.6)$$

where the additional term $\int \nu(\rho) |\nabla \mathbf{u}|^2 d\mathbf{x}$ in the dissipation can smooth the gradient, as in Laplacian smoothing gradient descent (Osher et al., 2018).

For a given energy-dissipation law, the energetic variational approach (Liu, 2009; Giga et al., 2017), originated from (Rayleigh, 1873) and (Onsager, 1931a;b), provides a unique way to determine the dynamics of a system through

Least Action Principle (LAP) and Maximum Dissipation Principle (MDP), that is

$$\frac{\delta \mathcal{D}}{\delta \phi_t} = - \frac{\delta \mathcal{F}}{\delta \phi}. \quad (2.7)$$

Equation (2.7) is known as the force balance equation. Its left-hand side corresponds to the dissipative force obtained from MDP, i.e., taking the variation of \mathcal{D} with respect to ϕ_t , and the right-hand side corresponds to conservative force obtained from LAP, i.e., taking the variation of $-\mathcal{F}$ with respect to ϕ . Recall that we let $\mathcal{F} = \text{KL}(\rho_{[\phi]} \parallel \rho^*)$ and $\mathcal{D} = \frac{1}{2} \int \eta(\rho_{[\phi]}) |\mathbf{u}|^2 d\mathbf{x}$. Applying the general energetic variational approach (2.7) to the (2.5), we can obtain

$$\eta(\rho) \mathbf{u} = - \frac{\delta \text{KL}}{\delta \phi}. \quad (2.8)$$

Let $V = -\ln \rho^*$ for short. By a direct computation (derivations in Supplement Materials), we have

$$- \frac{\delta \text{KL}(\rho_{[\phi]} \parallel \rho^*)}{\delta \phi} = -(\nabla \rho + \rho \nabla V). \quad (2.9)$$

Hence the transport velocity \mathbf{u} satisfies

$$\eta(\rho) \mathbf{u} = -(\nabla \rho + \rho \nabla V). \quad (2.10)$$

This equation gives us the specification of \mathbf{u} based on the energy-dissipation law. Thanks to the transport equation (2.11), ρ can be obtained from the specified \mathbf{u} . Therefore, (2.10) can be used to find the ρ that minimizes the KL-divergence. We call this framework *Energetic Variational Inference* (EVI).

When the flow map is defined by the velocity field $\mathbf{u}(\mathbf{x}, t)$, the corresponding distribution $\rho(\mathbf{x}, t)$ satisfies the transport equation

$$\begin{cases} \rho_t + \nabla \cdot (\rho \mathbf{u}) = 0, \\ \rho(\mathbf{x}, 0) = \rho_0(\mathbf{x}). \end{cases} \quad (2.11)$$

More precisely,

Theorem 2.1. *If $\phi^t(\mathbf{z})$ satisfies (2.3) and $\mathbf{x} = \phi^t(\mathbf{z})$, the time-dependent probability density $\rho(\mathbf{x}, t)$ induced by $\phi^t(\mathbf{z})$ satisfies the transport equation (2.11), where ρ_0 is the initial density and $\rho_t = \frac{\partial \rho(\mathbf{x}, t)}{\partial t}$.*

Proof of Theorem 2.1 is in the Supplied Materials. According to Theorem 2.1 and the velocity equation (2.10), we have

$$\rho_t = \nabla \cdot \left(\frac{\rho}{\eta(\rho)} (\nabla \rho + \rho \nabla V) \right), \quad (2.12)$$

which is the continuous differential equation formulation for ρ . One can choose $\eta(\rho)$ to control the dynamics of the system. In the remainder of the paper, we choose $\eta(\rho) = \rho$. Such an approach is consistent with the Wasserstein

gradient flow (Jordan et al., 1998; Santambrogio, 2017; Frogner & Poggio, 2018), in which the velocity is given by

$$\mathbf{u} = -\nabla \left(\frac{\delta \text{KL}(\rho || \rho^*)}{\delta \rho} \right) = - \left(\frac{1}{\rho} \nabla \rho + \nabla V \right). \quad (2.13)$$

3. Particle-based EVI

In practice, there are two ways to approximate a probability density in \mathcal{Q} defined in (2.1). One is to approximate the transport map $\phi(\mathbf{z}, t)$ directly, as used in variational inference with normalizing flow (Rezende & Mohamed, 2015). The transport map can be approximated either by a family of parametric transforms (Rezende & Mohamed, 2015) or a piece-wise linear map (Carrillo et al., 2018; Liu & Wang, 2019). The main difficulty in such approaches is how to compute $\det(\nabla_{\mathbf{z}} \phi(\mathbf{z}, t))$ efficiently. We refer readers to (Rezende & Mohamed, 2015), (Carrillo et al., 2018), and (Liu & Wang, 2019) for details.

Alternatively, a probability density in \mathcal{Q} can be approximated by an empirical measure defined by a set of sample points $\{\mathbf{x}_i(t)\}_{i=1}^N$. As used in many ParVI methods,

$$\rho(\mathbf{x}, t) \approx \rho_N^t(\mathbf{x}) = \frac{1}{N} \sum_{i=1}^N \delta(\mathbf{x} - \mathbf{x}_i(t)), \quad (3.1)$$

where $\mathbf{x}_i(t) = \phi(\mathbf{x}_i(0), t)$ and $\mathbf{x}_i(0)$ is sampled from the initial reference distribution ρ_0 . The sample points $\{\mathbf{x}_i(t)\}_{i=1}^N$ at time t are called ‘‘particles’’ in the ParVIs literature. Instead of computing the map $\phi(\mathbf{z}, t)$ explicitly at each time-step, only $\{\mathbf{x}_i(t)\}_{i=1}^N$ are computed in ParVIs.

3.1. Approximation-then-Variation v.s. Variation-then-Approximation

Using the proposed EVI framework, the evolution of particles $\{\mathbf{x}_i(t)\}_{i=1}^N$ can be characterized by a system of ODEs derived from the energy-dissipation law. There are two ways to get such an ODE system. For short, we call them ‘‘Approximation-then-Variation’’ and ‘‘Variation-then-Approximation’’ approaches. Essentially, the two approaches use different orders of density approximation and variational procedure, which lead to different ODE systems.

The **Approximation-then-Variation** approach starts with the discrete energy-dissipation law

$$\frac{d}{dt} \mathcal{F}_h(\{\mathbf{x}_i(t)\}_{i=1}^N) = -2\mathcal{D}_h(\{\mathbf{x}_i(t)\}_{i=1}^N, \{\mathbf{x}'_i(t)\}_{i=1}^N). \quad (3.2)$$

It can be obtained by inserting the empirical approximation (3.1) into the continuous energy-dissipation law with a suitable *kernel regularization*. For instance, a discrete version

of (2.5), which is the proposed dissipation mechanism of the KL-divergence, can be obtained by applying the particle approximation $\rho_N^t(\mathbf{x})$ to (2.5). To avoid $\ln \delta(\mathbf{x} - \mathbf{x}_i(t))$ operation, the kernel regularization we use is the convolution $K_h * \rho_N^t$ inside the \ln function. Here K_h is a kernel function. This particle-based approximation leads the regularized energy-dissipation law

$$\frac{d}{dt} \int \rho_N^t \ln(K_h * \rho_N^t) + V \rho_N^t d\mathbf{x} = - \int_{\Omega} \rho_N^t |\mathbf{u}|^2 d\mathbf{x}, \quad (3.3)$$

where

$$K_h * \rho_N^t(\mathbf{x}) = \int K_h(\mathbf{x} - \mathbf{y}) \rho_N^t(\mathbf{y}) d\mathbf{y} = \frac{1}{N} \sum_{j=1}^N K_h(\mathbf{x} - \mathbf{x}_j).$$

We denote $K_h(\mathbf{x} - \mathbf{x}_j)$ by $K_h(\mathbf{x}, \mathbf{x}_j)$, which is a more conventional notation in the literature. A typical choice of K_h is the Gaussian kernel

$$K_h(\mathbf{x}_1, \mathbf{x}_2) = \frac{1}{(\sqrt{2\pi}h)^d} \exp\left(-\frac{|\mathbf{x}_1 - \mathbf{x}_2|^2}{h^2}\right). \quad (3.4)$$

The regularized free energy (3.3) is proposed in (Carrillo et al., 2019) and has been used to design the Blob variational inference method in (Chen et al., 2018). By assuming $\mathbf{u}(\mathbf{x}_i(t)) \approx \mathbf{x}'_i(t)$, the discrete energy is

$$\begin{aligned} \mathcal{F}_h(\{\mathbf{x}_i\}_{i=1}^N) \\ = \frac{1}{N} \sum_{i=1}^N \left(\ln \left(\frac{1}{N} \sum_{j=1}^N K_h(\mathbf{x}_i, \mathbf{x}_j) \right) + V(\mathbf{x}_i) \right), \end{aligned} \quad (3.5)$$

and the discrete dissipation is

$$-2\mathcal{D}_h(\{\mathbf{x}_i\}_{i=1}^N) = -\frac{1}{N} \sum_{i=1}^N |\mathbf{x}'_i(t)|^2. \quad (3.6)$$

We can derive the equation of $\mathbf{x}'_i(t)$ via a discrete energetic variational approach (Liu & Wang, 2019)

$$\frac{\delta \mathcal{D}_h}{\delta \mathbf{x}'_i(t)} = -\frac{\delta \mathcal{F}_h}{\delta \mathbf{x}_i}, \quad (3.7)$$

which is the energetic variational approach performed at the particle level. An advantage of employing the discrete energetic variational approach is that the resulting system of $\mathbf{x}'_i(t)$'s preserves the variational structure at the particle level. The benefit of this property is discussed in Remark 3.3 in Section 3.2. By direct computation, we obtain a systems of ODEs for $\mathbf{x}_i(t)$ as

$$\begin{aligned} \mathbf{x}'_i(t) = & - \left(\frac{\sum_{j=1}^N \nabla_{\mathbf{x}_i} K_h(\mathbf{x}_i, \mathbf{x}_j)}{\sum_{j=1}^N K_h(\mathbf{x}_i, \mathbf{x}_j)} \right. \\ & \left. + \sum_{k=1}^N \frac{\nabla_{\mathbf{x}_i} K_h(\mathbf{x}_k, \mathbf{x}_i)}{\sum_{j=1}^N K_h(\mathbf{x}_k, \mathbf{x}_j)} + \nabla_{\mathbf{x}_i} V(\mathbf{x}_i) \right). \end{aligned} \quad (3.8)$$

It corresponds to the ODE system of the Blob method in (Chen et al., 2018). However, the derivation of (3.8) here is different from (Chen et al., 2018).

Remark 3.1. *Some more complicated forms of kernel regularization can be used in the approximation step. For instance, another regularized energy-dissipation law can be*

$$\begin{aligned} \frac{d}{dt} \int (K_h * \rho_N^t) \ln(K_h * \rho_N^t) + V \cdot (K_h * \rho_N^t) d\mathbf{x} \\ = - \int_{\Omega} (K_h * \rho_N^t) |\mathbf{u}|^2 d\mathbf{x}, \end{aligned}$$

but it may result in a more complicated particle equation.

The **Variation-then-Approximation** approach inserts the empirical approximation (3.1) to (2.10). Note that (2.10) is obtained after the variational step in (2.8). Thus variation step is done before the approximation step. Some kind of kernel regularization (Degond & Mustieles, 1990; Lacombe & Mas-Gallic, 1999) is needed because $\nabla \rho$ only exists when ρ is a valid distribution function, but ρ_N^t is not due to δ functions. Many existing ParVI methods belong to this category. Here are some examples.

As pointed out in (Liu, 2017) and (Lu et al., 2019), the ODE system corresponding to the standard SVGD is

$$\mathbf{x}'_i(t) = - \sum_{j=1}^N (K_h(\mathbf{x}_i, \mathbf{x}_j) \nabla V(\mathbf{x}_j) + \nabla_{\mathbf{x}_i} K_h(\mathbf{x}_i, \mathbf{x}_j)).$$

In fact, this ODE system can also be obtained using the EVI framework. Apply convolution to the right-hand side of (2.10) after replacing ρ by ρ_N^t by a kernel function K_h . We have

$$\rho_N^t \mathbf{u} = K_h * (\rho_N^t \nabla V + \nabla \rho_N^t),$$

which is the same as the ODE system of SVGD.

Another ParVI method is Gradient Flow with Smoothed test Function (GFSF), proposed by (Liu et al., 2019). Using the EVI framework, GFSF can be obtained by applying convolution to both side of (2.10) with a kernel function K_h

$$K_h * (\rho_N^t \mathbf{u}) = -K_h * (\rho_N^t \nabla V + \nabla \rho_N^t),$$

which gives us (let $K_{ij} = K_h(\mathbf{x}_i, \mathbf{x}_j)$ for short)

$$\sum_{j=1}^N K_{ij} \mathbf{x}'_j(t) = - \sum_{j=1}^N (K_{ij} \nabla V(\mathbf{x}_j) + \nabla_{\mathbf{x}_i} K_h(\mathbf{x}_i, \mathbf{x}_j)).$$

Although its right-hand is exactly the descent direction in SVGD, the left is different from SVGD.

The third ParVI method we discuss is Gradient Flow with Smoothed Density (GFSD), also proposed by (Liu et al.,

2019). Under the EVI framework, GFSD can be obtained by applying convolution to both the numerator and denominator of the first term in (2.13) with a kernel function K_h , i.e.,

$$\mathbf{u}(\mathbf{x}) = \frac{\rho_N^t * \nabla K_h}{\rho_N^t * K_h} - \nabla V(\mathbf{x}).$$

It leads to the same ODE system of the GFSD

$$\mathbf{x}'_i(t) = - \left(\frac{\sum_{j=1}^N \nabla_{\mathbf{x}_i} K_h(\mathbf{x}_i, \mathbf{x}_j)}{\sum_{j=1}^N K_h(\mathbf{x}_i, \mathbf{x}_j)} + \nabla V(\mathbf{x}_i) \right).$$

Remark 3.2. *There is another way to apply particle methods to solve the equation (2.12), known as the stochastic particle method, in which the diffusion term is approximated by Brownian motion. Such an approach is also known as the stochastic gradient Langevin dynamics (SGLD)*

$$\mathbf{x}'_i(t) = -\nabla V(\mathbf{x}_i) + \sqrt{2} dW_t$$

in Bayesian inference (Welling & Teh, 2011).

To sum up, EVI is a very general framework for variational inference, as exchanging the variation and approximation steps can lead to various different ODE systems of the particles and derive many existing and new ParVI methods. This is an appealing advantage of the proposed EVI.

3.2. Explicit v.s. Implicit

In this subsection, we adopt the ‘‘Approximation-then-Variation’’ approach to derive a new ParVI method. The ‘‘Approximation-then-Variation’’ approach leads to the ODE system (3.8). To solve it, one can use the explicit or implicit Euler method. Using the explicit Euler method, we can obtain the following numerical scheme

$$\frac{1}{N} \frac{\mathbf{x}_i^{n+1} - \mathbf{x}_i^n}{\tau_n} = - \frac{\mathcal{F}_h}{\delta \mathbf{x}_i} (\{\mathbf{x}_i^n\}_{i=1}^N), \quad (3.9)$$

where τ_n is the step-size. Here \mathcal{F}_h is the discrete KL-divergence defined in (3.5), and $\frac{\mathcal{F}_h}{\delta \mathbf{x}_i}$ is

$$\begin{aligned} \frac{\delta \mathcal{F}_h}{\delta \mathbf{x}_i} (\{\mathbf{x}_i^n\}_{i=1}^N) &= \frac{1}{N} \left(\frac{\sum_{j=1}^N \nabla_{\mathbf{x}_i} K_h(\mathbf{x}_i^n, \mathbf{x}_j^n)}{\sum_{j=1}^N K_h(\mathbf{x}_i^n, \mathbf{x}_j^n)} \right. \\ &\quad \left. + \sum_{k=1}^N \frac{\nabla_{\mathbf{x}_i} K_h(\mathbf{x}_k^n, \mathbf{x}_i^n)}{\sum_{j=1}^N K_h(\mathbf{x}_k^n, \mathbf{x}_j^n)} + \nabla_{\mathbf{x}_i} V(\mathbf{x}_i^n) \right). \end{aligned}$$

Scheme (3.9) is exactly the Blob scheme proposed in (Chen et al., 2018). The explicit Euler scheme is used to solve various ODE systems of the particles in many other existing ParVI methods (Liu & Wang, 2016; Chen et al., 2018; Liu & Zhu, 2018; Liu et al., 2019). In the implementation of these methods, AdaGrad (Duchi et al., 2011) is often used to update the step-size. Although these algorithms

perform well in practice, the AdaGrad scales each component of the updating direction differently. As a result, the updating directions of these algorithms are in fact different from their original ODE systems.

An alternative approach is to adopt the implicit Euler scheme for the temporal discretization, i.e.,

$$\frac{1}{N} \frac{\mathbf{x}_i^{n+1} - \mathbf{x}_i^n}{\tau} = -\frac{\delta \mathcal{F}_h}{\delta \mathbf{x}_i}(\{\mathbf{x}_i^{n+1}\}_{i=1}^N). \quad (3.10)$$

The equations (3.10) for $i = 1, \dots, N$ form a system of nonlinear equations. To solve them, we first define

$$J_n(\{\mathbf{x}_i\}_{i=1}^N) = \frac{1}{2\tau} \sum_{i=1}^N |\mathbf{x}_i - \mathbf{x}_i^n|^2 / N + \mathcal{F}_h(\{\mathbf{x}_i\}_{i=1}^N). \quad (3.11)$$

It is easy to see that (3.10) is the gradient of $J_n(\{\mathbf{x}_i\}_{i=1}^N)$ with respect to the vectorized $\{\mathbf{x}_i\}_{i=1}^N$ (See the proof of Theorem 3.1). Therefore, we can solve the nonlinear equations by solving the optimization problem.

$$\{\mathbf{x}_i^{n+1}\}_{i=1}^N = \operatorname{argmin}_{\{\mathbf{x}_i\}_{i=1}^N} J_n(\{\mathbf{x}_i\}_{i=1}^N). \quad (3.12)$$

The optimization problem (3.12) can be solved by a suitable nonlinear optimization method. Following (Braides, 2014) and (Carrillo et al., 2019), we can prove Theorem 3.1.

Theorem 3.1. *For a sufficient smooth target distribution ρ^* and any given $\{\mathbf{x}_i^n\}_{i=1}^N$, there exists at least one minimal solution of (3.12) $\{\mathbf{x}_i^{n+1}\}_{i=1}^N$ that also satisfies*

$$\frac{\mathcal{F}_h(\{\mathbf{x}_i^{n+1}\}_{i=1}^N) - \mathcal{F}_h(\{\mathbf{x}_i^n\}_{i=1}^N)}{\tau} \leq -\sum_{i=1}^N \frac{|\mathbf{x}_i^{n+1} - \mathbf{x}_i^n|^2}{2N\tau^2}. \quad (3.13)$$

Moreover, as n increases, keep updating $\{\mathbf{x}_i^n\}_{i=1}^N$ by $\{\mathbf{x}_i^{n+1}\}_{i=1}^N$ which also satisfies (3.13). The series $\{\mathbf{x}_i^n\}$ converges to a stationary point of $\mathcal{F}_h(\{\mathbf{x}_i\}_{i=1}^N)$ as $n \rightarrow \infty$.

Theorem 3.1 guarantees the existence of a solution of (3.10) that also decreases the discrete KL-divergence in each iteration. We define using the implicit Euler scheme to solve (3.8) as Algorithm 1.

Algorithm 1 EVI with Implicit Euler Scheme (EVI-Im)

Input: The target distribution $\rho^*(\mathbf{x})$ and a set of initial particles $\{\mathbf{x}_i^0\}_{i=1}^N$ drawn from a prior $\rho_0(\mathbf{x})$.

Output: A set of particles $\{\mathbf{x}_i^*\}_{i=1}^N$ approximating ρ^* .

for $n = 0$ **to** MaxIter **do**

Solve $\{\mathbf{x}_i^{n+1}\}_{i=1}^N = \operatorname{argmin}_{\{\mathbf{x}_i\}_{i=1}^N} J_n(\{\mathbf{x}_i\}_{i=1}^N)$.

Update $\{\mathbf{x}_i^n\}_{i=1}^N$ by $\{\mathbf{x}_i^{n+1}\}_{i=1}^N$.

end for

The inequality (3.13) does not automatically hold for any local minimal solution of (3.12) unless this solution is also

the global minimal solution. However, the convexity of the objective function is not clear, and in practice, it is difficult to obtain the exact global minimizer of $J_n(\{\mathbf{x}_i\}_{i=1}^N)$ via most existing nonlinear optimization methods. Therefore, (3.13) should be checked in each iteration to make sure Algorithm 1 converges. But it is too time-consuming to do so as it needs to compute $\mathcal{F}_h(\{\mathbf{x}_i\}_{i=1}^N)$. In Algorithm 1, we adopt the gradient descent with Barzilai-Borwein step size (Barzilai & Borwein, 1988). Numerical experiments have shown that such algorithm usually can find a stationary point of $J_n(\{\mathbf{x}_i\}_{i=1}^N)$ that also satisfies (3.13) with relatively small value of τ .

Remark 3.3. *Although the implicit Euler scheme can also be applied to solve the ODEs obtained by the Variation-then-Approximation approach, it is difficult to convert the resulting system of nonlinear equations to an optimization problem, since it is unclear whether the right-hand of these equations correspond to the gradients of some functions, i.e., the variational structure at the particle level. An advantage of the Approximation-then-Variation approach is that the variational structure is naturally preserved at the particle level. In other words, the right-hand side of the ODE system (3.7), $\frac{\delta \mathcal{F}_h}{\delta \mathbf{x}_i}$, is always the gradient of $\mathcal{F}_h(\{\mathbf{x}_i\}_{i=1}^N)$ with respect to the vectorized $\{\mathbf{x}_i\}_{i=1}^N$. Hence, we can formulate the implicit Euler scheme as an optimization problem.*

Using Algorithm 1, we update the position of particles by closely following the continuous energy-dissipation law, which provides an efficient way to push the particles to follow the target distribution. In practice, it is not necessary to obtain a minimizer of $J_n(\{\mathbf{x}_i\}_{i=1}^N)$ at each iteration. In fact, we only need to find $\{\mathbf{x}_i^{n+1}\}_{i=1}^N$ such that

$$\mathcal{F}_h(\{\mathbf{x}_i^{n+1}\}) \leq \mathcal{F}_h(\{\mathbf{x}_i^n\}),$$

which usually can be achieved in a few steps via the gradient descent method or Newton-like methods with suitable step sizes to $J_n(\{\mathbf{x}_i\}_{i=1}^N)$. One can even adopt a line search procedure to guarantee that $J_n(\{\mathbf{x}_i^{n+1}\}_{i=1}^N) \leq J_n(\{\mathbf{x}_i^n\}_{i=1}^N)$.

This optimization perspective can also lead to other ParVI methods. For example, the previously mentioned the Blob method (without AdaGad) uses the explicit Euler scheme to solve the ODE system, and it is the same as doing one gradient descent step to decrease $J_n(\{\mathbf{x}_i\}_{i=1}^N)$, and the idea of Stein Variational Newton (SVN) type algorithms (Detommaso et al., 2018; Chen et al., 2019) is the same as doing one Newton step to decrease $J_n(\{\mathbf{x}_i\}_{i=1}^N)$.

High-order temporal discretization can also be used to solve (3.8), such as the Crank-Nicolson scheme and BDF2 (Iserles, 2009). Within the variational structure at the particle level, these schemes can also be formulated into opti-

mization problems (Matthes & Plazotta, 2019; Du & Feng, 2019).

3.3. Choice of Kernel

We briefly discuss the choice of kernel, or more precisely, the choice of bandwidth h . The role of kernel function $K_h(\mathbf{x} - \mathbf{x}_i)$ is essentially to approximate $\delta(\mathbf{x} - \mathbf{x}_i)$. Considering this role, h should be as small as possible when the number of particles is large. However, in practice, since the number of particles is finite, it is not clear how small h should be.

Intuitively, for Gaussian kernel, h controls the inter-particle distances. In the original SVGD (Liu & Wang, 2016), the bandwidth is set to be $h = \text{med}^2 / \log N$ where med is the median of the pairwise distance between the current particles. The median trick updates the bandwidth after each iteration. Recently, a matrix-valued kernel for SVGD has been proposed in (Wang et al., 2019). It selects the optimal bandwidth via Fisher information.

The optimal bandwidth and the choice of kernel function are problem-dependent. Sometimes, a non-Gaussian kernel might be better (Francois et al., 2005). We do not intend to further the discussion here. In our examples, we fix the bandwidth of the Gaussian kernel by conducting multiple trials. The results show that fixed kernel bandwidth works well in many situations for the proposed Algorithm 1.

4. Experiments

We compare the proposed EVI scheme summarized in Algorithm 1 (or EVI-Im for short) with some other ParVI methods on two synthesized examples (Example 1 and 2) and one example with real data (Example 3). The methods we have compared include AdaGrad based classical SVGD (Liu & Wang, 2016), matrix-valued SVGD (Liu et al., 2019), Riemannian SVGD (Liu & Zhu, 2018), and Blob method (Chen et al., 2018). Additional examples are included in Supplement Materials.

In Example 1, because the posterior distribution (i.e., the target distribution) is known, we can calculate the cross-entropy defined as $E_{\mathbf{x} \sim \rho^*}(-\ln \rho^*(\mathbf{x})) \approx -\frac{1}{N} \sum_{i=1}^N \ln \rho^*(\mathbf{x}_i)$ as the criterion to compare different methods. Here ρ^* is the known posterior distribution and \mathbf{x}_i 's are the positions of the particles. For Example 2, the exact posterior distribution is not available, thus we only compare the EVI-Im method with the classic SVGD visually. In Example 3, the Bayesian logistic regression model is trained on the real data, we can calculate the likelihood of the training data sets and the classification accuracy on the test data sets.

In EVI-Im, the number of iterations is n defined in the loop

in Algorithm 1. Therefore, one iteration leads to one update of the positions of the particles. We need to point out that the amount of computation in one iteration of the EVI-Im method is much larger than the other ParVI methods discussed here. The reason is that the minimization problem (3.12) needs to be solved in each iteration of EVI-Im. The optimization normally takes less than 100 iterations to reach convergence on average.

Example 1. Star-Shaped Distribution. We use the same two-dimensional synthesized example studied in (Wang et al., 2019). The posterior is given as a star-shaped the probability function, and the contour plot of the density function is plotted in Fig. 1 (a).

We compare three methods, the EVI-Im ($\tau = 0.1$), the Blob method with AdaGrad (lr = 0.5), and the matrix-valued SVGD (mixture, lr = 0.5). For the Blob method and matrix-valued SVGD, the learning rate is chosen as the best one after many trials. We use $N = 200$ particles and the same initial set of particles sampled from the 2-dim standard normal distribution in all methods. For the EVI-Im and the Blob method, we fix the kernel bandwidth to be $h = 0.1$. The bandwidth matrix in the matrix-valued SVGD is set as the exact Hessian matrices as in (Wang et al., 2019). The results are shown in Fig. 1. We observe that the proposed EVI-Im method and the Blob method reach smaller cross-entropy than the matrix-valued SVGD when the algorithms converge, which means that the empirical distribution of the particles returned by EVI-Im and Blob methods are closer to the target distribution than that of matrix-valued SVGD. Since the Blob and the EVI-Im methods minimize the same discrete KL-divergence defined in (3.5), their results are similar.

Although the Blob method with AdaGrad approximates the posterior relatively well, the cross-entropy of the Blob method keeps oscillating, especially during the early stage of iterations. Using the EVI-Im, we can obtain a good approximation within less than 20 iterations with $\tau = 0.1$, although the computation cost of each iteration of EVI-Im is much larger than the AdaGrad-based Blob since the optimization problem (3.12) is solved in each iteration.

Example 2. Gaussian Mixture Model. This example is about a simple but interesting Gaussian Mixture Model (GMM) following the same settings as in (Dai et al., 2016) and (Welling & Teh, 2011). We sample 1000 observed data from $\mathbf{y} \sim \frac{1}{2}(N(\omega_1, \sigma^2) + N(\omega_1 + \omega_2, \sigma^2))$, where $(\omega_1, \omega_2) = (1, -2)$ and $\sigma = 2.5$. Using the conjugate prior $\omega_1, \omega_2 \sim N(0, 1)$, the posterior distribution is a Gaussian mixture distribution with two modes, $(1, -2)$ and $(-1, 2)$. We have tried the SVGD with learning rate lr = 0.01, 0.1, 0.5, 1.0 and choose the best learning rate lr = 1. For EVI-Im, we set $\tau = 0.01$. The same $N = 100$ initial particles sampled from the prior are used in both

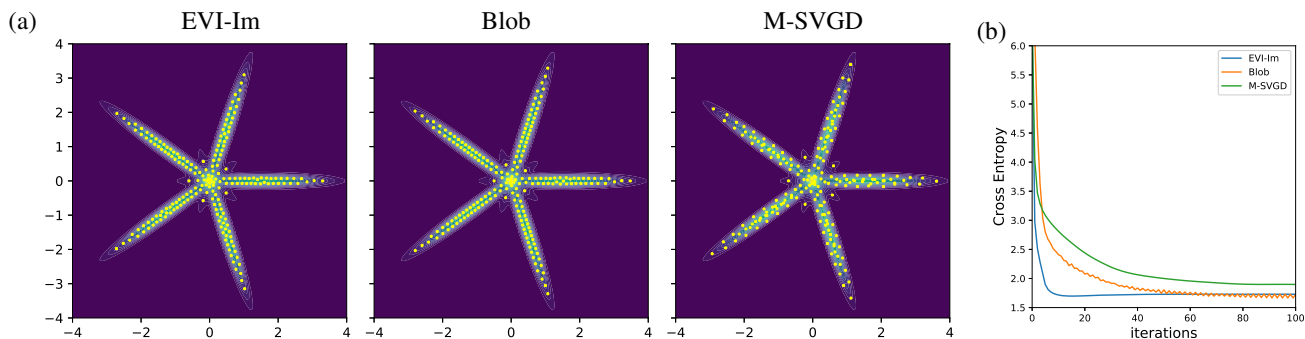


Figure 1: Example 1. (a) Particles obtained by various methods [200 particles]: EVI-Im after 20 iterations, Blob method and matrix-valued SVGD both after 1000 iterations; (b) cross-entropy v.s. number of iterations of the three methods.

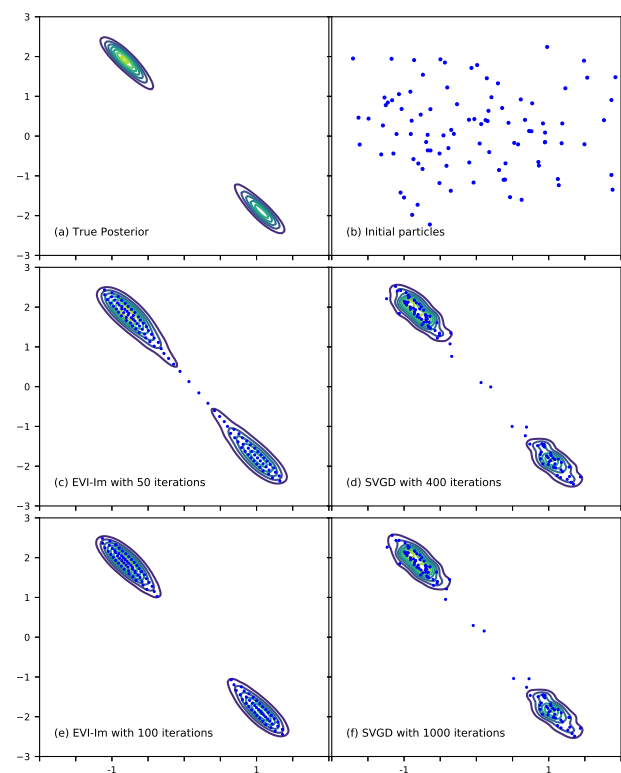


Figure 2: Comparison of EVI-Im and the classic SVGD ($lr = 1$) at different iterations in Example 2.

methods.

Figure 2 shows the posterior distribution approximated by EVI-Im and SVGD ($lr = 1.0$). Kernel density estimation with optimal bandwidth selected via cross-validation is used to generate the estimated posterior distribution for both methods. Fig. 2 shows the approximated distributions of EVI-Im and SVGD at different iterations. When both methods converge, EVI-Im (100 iterations) approximates the true posterior distribution better than the SVGD (1000 iterations). In the middle of the procedure, the particles of

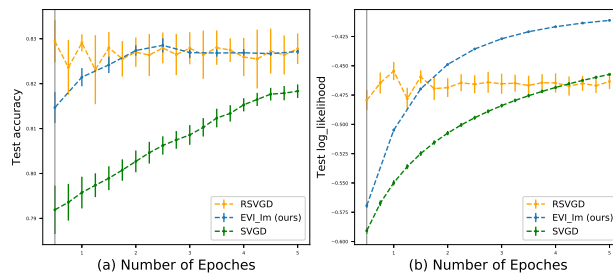


Figure 3: Example 3. The test accuracy and log-likelihood of the training data (20 simulations) returned by EVI-Im, RSVGD, and SVGD methods.

the EVI-Im also appear to be aligned more regularly. But among the particles returned by SVGD, some are clustered and some are scattered widely. The EVI-Im is also comparable with other methods in (Dai et al., 2016).

Example 3. Bayesian Logistic Regression with Real Data.

We apply the Bayesian logistic regression model to the data set SPLICE (1,000 training entries, 60 features), a benchmark data set used in (Mika et al., 1999) and (Liu & Zhu, 2018). The unknown parameters ω are the regression coefficients following, whose prior is $N(\omega; 0, \alpha I)$. We compare the EVI-Im method with the classic SVGD and the Riemannian SVGD (RSVGD) (Liu & Zhu, 2018). For the latter two, we use the codes¹ by (Liu & Zhu, 2018). We compute the test accuracy and log-likelihood of the training data for all methods at different epoch for a fair comparison,. An epoch is defined as 100 iterations is SVGD and RSVGD. The amount of computation of one epoch for SVGD and RSVGD can be roughly considered as the amount of one iteration for the EVI-Im.

Figure 3 shows the comparisons of test accuracy and log-likelihood of the three methods, The mean and standardization of 20 simulations of the two measures are plotted. Each simulation uses newly sampled initial particles for all

¹<https://github.com/changliu00/Riem-SVGD>

methods. In terms of the test accuracy, EVI-Im is not as good as the RSVGd initially, but the two perform similarly when they both reach convergence. In terms of the log-likelihood, EVI-Im performs the best. Although RSVGd can obtain high test accuracy in a few epochs, its log-likelihood of the training data remains low. The proposed EVI-Im returns comparable test accuracy with RSVGd and is less sensitive to the initial particle values.

5. Conclusion

In this paper, we introduce a new variational inference framework, called energetic variational inference (EVI). Inspired by the *energy-dissipation law* from physics, EVI minimizes the KL-divergence by employing an energetic variational approach. The EVI is a general framework, as many existing and new flow-based variational inference methods can be derived from it. Here we have derived one particle-based EVI method using the ‘Approximation-then-Variation’ order, and the resulting ODE system is solved by the implicit Euler scheme. Numerical examples show that the proposed method has comparable performance with the latest ParVI methods. As discussed in several Remarks, different combinations of energy-dissipation laws, the orders of approximation and variation, and numerical schemes for ODEs can lead to many new variational inference methods. This opens doors to many varieties in the variational inference literature.

A. Proof

A.1. Proof of Theorem 2.1

Proof. The transport equation can be derived from conservation of probability mass directly. Let

$$F(\mathbf{z}, t) = \nabla_{\mathbf{z}} \phi(\mathbf{z}, t), \quad (\text{A.1})$$

then due to the conservation of probability mass, we have

$$\begin{aligned} 0 &= \frac{d}{dt} \int_{\mathcal{X}^t} \rho(\mathbf{x}, t) d\mathbf{x} = \frac{d}{dt} \int_{\mathcal{X}^0} \rho(\phi(\mathbf{z}, t), t) \det(F(\mathbf{z}, t)) d\mathbf{z} \\ &= \int_{\mathcal{X}^0} \left(\rho_t + \nabla \rho \cdot \mathbf{u} + \rho(F^{-T} : \frac{dF}{dt}) \right) \det F d\mathbf{z} \\ &= \int_{\mathcal{X}^t} (\rho_t + \nabla \rho \cdot \mathbf{u} + \rho(\nabla \cdot \mathbf{u})) d\mathbf{x} = 0, \end{aligned}$$

which implies that

$$\rho_t + \nabla \cdot (\rho \mathbf{u}) = 0. \quad (\text{A.2})$$

□

A.2. Computation of Equation (2.10)

In this part, we give a detailed derivation of the variation of $\text{KL}(\rho_{[\phi]} || \rho^*)$ with respect to the flow map $\phi(\mathbf{z}) : \mathcal{X}^0 \rightarrow$

\mathcal{X}^t . Consider a small perturbation of ϕ

$$\phi^\epsilon(\mathbf{z}) := \phi(\mathbf{z}) + \epsilon \psi(\mathbf{z}),$$

where $\psi(\mathbf{z}) = \tilde{\psi}(\phi(\mathbf{z}))$ is a smooth map satisfying

$$\tilde{\psi} \cdot \boldsymbol{\nu} = 0, \quad \text{on } \partial \mathcal{X}^t$$

with $\boldsymbol{\nu}$ be the outer norm of $\partial \mathcal{X}^t$. For $\mathcal{X}^0 = \mathcal{X}^d = \mathbb{R}^d$, $\tilde{\psi} \in C_0^\infty(\mathbb{R}^d)$. We denote

$$F^\epsilon := \nabla_{\mathbf{z}} \phi + \epsilon \nabla_{\mathbf{z}} \psi.$$

Then we have

$$\begin{aligned} &\frac{d}{d\epsilon} \Big|_{\epsilon=0} \text{KL}(\rho_{[\phi^\epsilon]} || \rho^*) \\ &= \frac{d}{d\epsilon} \Big|_{\epsilon=0} \left(\int_{\mathcal{X}^0} \frac{\rho_0}{\det F^\epsilon} \ln \left(\frac{\rho_0}{\det F^\epsilon} \right) \det(F^\epsilon) d\mathbf{z} \right. \\ &\quad \left. + \int_{\mathcal{X}^0} V(\phi^\epsilon(\mathbf{z}, t)) \rho_0 d\mathbf{z} \right) \\ &= \int_{\mathcal{X}^0} -\rho_0 (F^{-T} : \nabla_{\mathbf{z}} \psi) + (\nabla V \cdot \psi) \rho_0 d\mathbf{z}. \end{aligned} \quad (\text{A.3})$$

After pushing back to \mathcal{X}^t and performing integration by parts, we have

$$\begin{aligned} &\frac{d}{d\epsilon} \Big|_{\epsilon=0} \text{KL}(\rho_{[\phi^\epsilon]} || \rho^*) \\ &= \int_{\mathcal{X}^t} -\rho_{[\phi]} (\nabla_{\mathbf{x}} \cdot \tilde{\psi}) + \rho \nabla V \cdot \tilde{\psi} d\mathbf{x} \\ &= \int_{\mathcal{X}^t} (\nabla \rho + \rho \nabla V) \cdot \tilde{\psi} d\mathbf{x}. \end{aligned}$$

Hence,

$$\frac{\delta \text{KL}(\rho_{[\phi]} || \rho^*)}{\delta \phi} = \nabla \rho + \rho \nabla V \quad (\text{A.4})$$

Recall $V = -\ln \rho^*$, one can notice that if F is a identity matrix, the result in (A.3) can be written as

$$-\mathbb{E}_{\mathbf{z} \sim \rho_0} [\text{trace}(\nabla_{\mathbf{z}} \psi + \nabla \ln \rho^* \psi^T)],$$

which is exactly the form given by the Stein operator in (Liu & Wang, 2016).

A.3. Proof of Theorem 3.1

The proof directly follows the procedure in (Braides, 2014; Carrillo et al., 2019).

Proof. Let $\mathbf{X} \in \mathbb{R}^D$ be vectorized $\{\mathbf{x}_i\}_{i=1}^N$, that is

$$\mathbf{X} = (x_1^{(1)}, \dots, x_N^{(1)}, \dots, x_1^{(d)}, \dots, x_N^{(d)}),$$

where $D = N \times d$.

Recall that $V(\mathbf{x}) = -\ln \rho^*$. For a sufficient smooth target distribution $\rho^*(\mathbf{x})$, it is easy to show that

$$\mathcal{F}_h(\{\mathbf{x}_i\}) = \frac{1}{N} \sum_{i=1}^N \left(\ln \left(\frac{1}{N} \sum_{j=1}^N K(\mathbf{x}_i, \mathbf{x}_j) \right) + V(\mathbf{x}_i) \right)$$

is continuous, coercive and bounded from below as a function of \mathbf{X} . We denote $\mathcal{F}_h(\{\mathbf{x}_i\})$ by $\mathcal{F}_h(\mathbf{X})$.

For any given $\{\mathbf{x}_i^n\}_{i=1}^N$, recall

$$J_n(\mathbf{X}) = \frac{1}{2\tau} \|\mathbf{X} - \mathbf{X}^n\|^2 + \mathcal{F}_h(\mathbf{X}),$$

where $\mathbf{X}^n \in \mathbb{R}^D$ is the vectorized $\{\mathbf{x}_i^n\}_{i=1}^N$, and $\|\cdot\|^2$ is defined by

$$\|\mathbf{X} - \mathbf{X}^n\|^2 = \frac{1}{N} \sum_{i=1}^N |\mathbf{x}_i - \mathbf{x}_i^n|^2.$$

Since

$$\mathcal{S} = \{J(\mathbf{X}) \leq J(\mathbf{X}^n)\}$$

is a non-empty, bounded, and closed set, by the coerciveness and continuity of $\mathcal{F}_h(\mathbf{X})$, $J_n(\mathbf{X})$ admits a global minimizer \mathbf{X}^{n+1} in \mathcal{S} . Since \mathbf{X}^{n+1} is a global minimizer of $J(\mathbf{X})$, we have

$$\frac{1}{2\tau} \|\mathbf{X}^{n+1} - \mathbf{X}^n\|^2 + \mathcal{F}_h(\mathbf{X}^{n+1}) \leq \mathcal{F}_h(\mathbf{X}^n),$$

which gives us equation (3.13).

For series $\{\mathbf{X}^n\}$, since

$$\|\mathbf{X}^k - \mathbf{X}^{k-1}\|^2 \leq 2\tau(\mathcal{F}_h(\mathbf{X}^{k-1}) - \mathcal{F}_h(\mathbf{X}^k)),$$

we have

$$\sum_{k=1}^n \|\mathbf{X}^k - \mathbf{X}^{k-1}\|^2 \leq 2\tau(\mathcal{F}_h(\mathbf{X}^0) - \mathcal{F}_h(\mathbf{X}^n)) \leq C,$$

for some constant C that is independent with n . Hence

$$\lim_{n \rightarrow \infty} \|\mathbf{X}^n - \mathbf{X}^{n-1}\| = 0,$$

which indicates the convergence of $\{\mathbf{X}^n\}$. Moreover, since

$$\mathbf{X}^n = \mathbf{X}^{n-1} - \tau \nabla_{\mathbf{X}} \mathcal{F}_h(\mathbf{X}^n),$$

we have

$$\lim_{n \rightarrow \infty} \nabla_{\mathbf{X}} \mathcal{F}_h(\mathbf{X}^n) = 0,$$

so $\{\mathbf{X}^n\}$ converges to a stationary point of $\mathcal{F}_h(\mathbf{X})$. \square

B. More experimental results

In this section, we provide more experimental results that compare EVI-Im with other ParVI methods.

B.1. Toy examples

We show three toy examples that are widely tested in previous variational inference methods (Rezende & Mohamed, 2015; Chen et al., 2018; Liu et al., 2019). All target distributions are specified in the examples, and EVI-Im algorithm is used to approximate the target distributions. The initial particles are sampled from 2-dim standard Gaussian distribution.

The first example is modified from (Haario et al., 1999). The target distribution is given by

$$\rho(\mathbf{x}) \propto \exp \left\{ -\frac{x_1^2}{2} - \frac{1}{2}(10x_2 + 3x_1^2 - 3)^2 \right\}.$$

The second example is similar to the examples tested in (Rezende & Mohamed, 2015; Liu et al., 2019). The target distribution has two component, given by

$$\rho(\mathbf{x}) \propto \exp \left\{ -2(\|\mathbf{x}\|_2^2 - 3)^2 + \log \left(e^{-2(x_1-3)^2} + e^{-2(x_1+3)^2} \right) \right\}.$$

The third example is from (Rezende & Mohamed, 2015) and (Chen et al., 2018).

$$\rho(\mathbf{x}) \propto \exp \left\{ -\frac{1}{2} \left[\frac{x_2 - \sin(\frac{\pi x_1}{2})}{0.4} \right]^2 \right\}.$$

We use $N = 50$ particles for the first example and $N = 120$ particles for the second and third examples. The bandwidth of the kernel is taken to be 0.05 for the first and second example, and 0.2 for the third example. We set $\tau = 0.01$ for all examples. Fig. 4 shows that the particles returned by the EVI-Im well approximate the target distributions. The second example is the most challenging one and requires more iterations because the support region (where the density is significantly larger than 0) of the target distribution is not connected and contains two banana shaped areas.

B.2. Coverttype Example

In this example, we compare the proposed EVI-Im algorithm and the original SVGD method on the data set Coverttype (Wang et al., 2019), which contains $S = 581,012$ data entries and 54 features. Denote the data entries by $\{\mathbf{x}_i, y_i\}_{i=1}^S$. In (Wang et al., 2019), a logistic regression model $p(y_i = 1 | \mathbf{x}_i, \boldsymbol{\omega}) = \frac{1}{1 + \exp(-\boldsymbol{\omega}^T \mathbf{x}_i)}$ is used to fit the data. The unknown parameters $\boldsymbol{\omega}$ are the regression coefficients and its prior is chosen to be $p(\boldsymbol{\omega}) = N(\boldsymbol{\omega}; 0, I)$.

We have run total 20 simulations and in each simulation we randomly partition the data into training (80% of the whole) and testing (20% of the whole) sets. Recall that in the EVI-Im algorithm, we need to solve a minimization problem in order to update the positions of the particles.

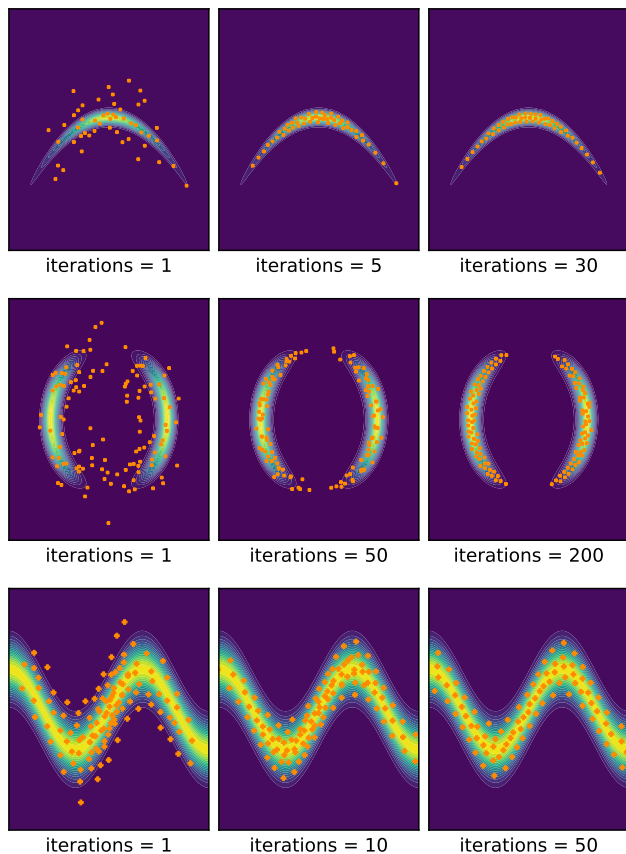


Figure 4: The particles obtained by EVI-Im algorithm approximating three target distributions plotted as contours.

Due to the large size of the data, it is not practical to still use the gradient descent with Barzilai-Borwein step size (Barzilai & Borwein, 1988) to achieve the local optimality. Here we choose the stochastic gradient descent method AdaGrad (Duchi et al., 2011), which is also used by various SVGD methods. We set the maximum number of iterations for the inner loop of AdaGrad to be 100 in the EVI-Im algorithm. Meanwhile, τ is set to be 0.1 in the EVI-Im algorithm. For the SVGD method, we choose the best learning rate from $[0.01, 0.05, 0.1, 0.5, 1.0]$. The batch size of AdaGrad used in both EVI-Im and SVGD is set to be 256. For all methods, we use $N = 20$ particles.

In statistical analysis of real data, it is a common practice to standardize all columns of inputs via their individual mean and standard deviation in the data preprocessing stage. Thus, we apply both EVI-Im and the SVGD algorithms to the standardized data. As baseline, we also apply the SVGD to the non-standardized data, which was done in the same way as in (Wang et al., 2019). The SVGD is implemented using the codes² by (Wang et al., 2019). Fig.

5 shows the accuracy of the classification of EVI-Im and SVGD applied to standardized data and SVGD applied to non-standardized data. The accuracy is the average of 20 simulations.

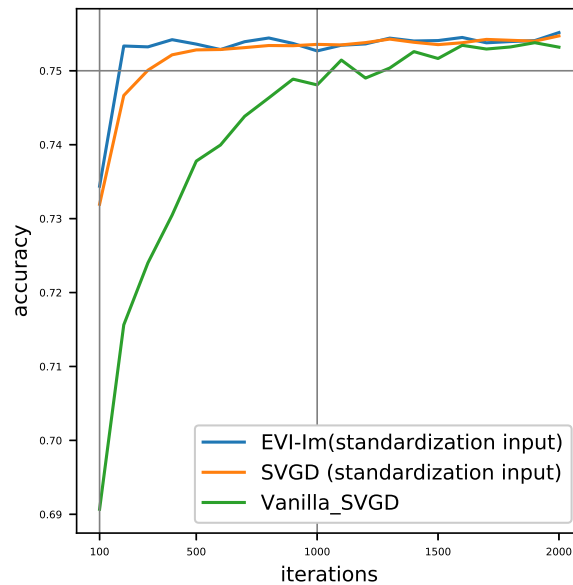


Figure 5: The accuracy of 20 simulations for Bayesian logistic regression on Covertype dataset using different methods.

From Fig. 5, we can first conclude that standardization significantly improves the accuracy of the SVGD method. This is expected because standardization is essentially applying different bandwidth values to different input dimensions inside the kernel function. As a result, the original SVGD with standardization performs similarly as the matrix-valued SVGD proposed in (Wang et al., 2019), although the latter also linearly transforms the SVGD direction by multiplying a precondition matrix on the original SVGD direction. For the same reason, EVI-Im algorithm also benefits from the standardization, as it is also a kernel-based method.

In Fig. 5, the accuracy of each method is plotted against number of iterations. For the SVGD, the number of iterations counts the iterations of the only layer of loop. For the SVI-Im, there are inner and outer loops, and the number of iterations counts the iterations from both, i.e., No. of Iterations = No. of Outer Iterations \times 100 (No. of Inner Iterations). Since both methods used the AdaGrad with the same batch size, Fig. 5 fairly compares how fast each method can achieve the best accuracy. Clearly, the proposed EVI-Im is the best among the three in this sense. We can also compare the EVI-Im algorithm with the matrix-valued SVGD. (Wang et al., 2019) shows that the matrix-valued SVGD can reach an accuracy of 0.75 in less than

²available from <https://github.com/dilinwang820/Standardized-SVGDI>

500 iterations. Using the EVI-Im algorithm with standardized data, we can the same 0.75 accuracy around 200 iterations.

At last, we point out that the proposed EVI-Im algorithm, the SVGD with or without standardized data, and the matrix-valued SVGD method have similar performance when they reach convergence. A major reason is that due to the large size of the data the KL-divergence is entirely dominated by the log-likelihood. Consequently, the interactions between particles play little effect in the updating of the particles. Thus, there is no significant distinction between different methods when they all reach convergence.

References

- Barzilai, J. and Borwein, J. M. Two-point step size gradient methods. *IMA journal of numerical analysis*, 8(1):141–148, 1988.
- Blei, D. M., Kucukelbir, A., and McAuliffe, J. D. Variational inference: A review for statisticians. *Journal of the American Statistical Association*, 112(518):859–877, 2017.
- Braides, A. *Local minimization, variational evolution and [gamma]-convergence*, volume 2094. Springer, 2014.
- Carrillo, J. A., Düring, B., Matthes, D., and McCormick, D. S. A lagrangian scheme for the solution of nonlinear diffusion equations using moving simplex meshes. *Journal of Scientific Computing*, 75(3):1463–1499, 2018.
- Carrillo, J. A., Craig, K., and Patacchini, F. S. A blob method for diffusion. *Calculus of Variations and Partial Differential Equations*, 58(2):53, 2019.
- Chen, C., Zhang, R., Wang, W., Li, B., and Chen, L. A unified particle-optimization framework for scalable bayesian sampling. *arXiv preprint arXiv:1805.11659*, 2018.
- Chen, P., Wu, K., Chen, J., O’Leary-Roseberry, T., and Ghattas, O. Projected stein variational newton: A fast and scalable bayesian inference method in high dimensions. *arXiv preprint arXiv:1901.08659*, 2019.
- Dai, B., He, N., Dai, H., and Song, L. Provable bayesian inference via particle mirror descent. In *Artificial Intelligence and Statistics*, pp. 985–994, 2016.
- Degond, P. and Mustieles, F.-J. A deterministic approximation of diffusion equations using particles. *SIAM Journal on Scientific and Statistical Computing*, 11(2):293–310, 1990.
- Detommaso, G., Cui, T., Marzouk, Y., Spantini, A., and Scheichl, R. A stein variational newton method. In *Advances in Neural Information Processing Systems*, pp. 9169–9179, 2018.
- Du, Q. and Feng, X. The phase field method for geometric moving interfaces and their numerical approximations. *arXiv preprint arXiv:1902.04924*, 2019.
- Duchi, J., Hazan, E., and Singer, Y. Adaptive subgradient methods for online learning and stochastic optimization. *Journal of Machine Learning Research*, 12(Jul): 2121–2159, 2011.
- El Moselhy, T. A. and Marzouk, Y. M. Bayesian inference with optimal maps. *Journal of Computational Physics*, 231(23):7815–7850, 2012.
- Francois, D., Wertz, V., Verleysen, M., et al. About the locality of kernels in high-dimensional spaces. In *International Symposium on Applied Stochastic Models and Data Analysis*, pp. 238–245. Citeseer, 2005.
- Frogner, C. and Poggio, T. Approximate inference with wasserstein gradient flows. *arXiv preprint arXiv:1806.04542*, 2018.
- Gelman, A., Carlin, J. B., Stern, H. S., Dunson, D. B., Vehtari, A., and Rubin, D. B. *Bayesian data analysis*. Chapman and Hall/CRC, 2013.
- Geman, S. and Geman, D. Stochastic relaxation, gibbs distributions, and the bayesian restoration of images. *IEEE Transactions on pattern analysis and machine intelligence*, PAMI-6(6):721–741, 1984.
- Giga, M.-H., Kirshtein, A., and Liu, C. Variational modeling and complex fluids. *Handbook of mathematical analysis in mechanics of viscous fluids*, pp. 1–41, 2017.
- Haario, H., Saksman, E., and Tamminen, J. Adaptive proposal distribution for random walk metropolis algorithm. *Computational Statistics*, 14(3):375–396, 1999.
- Hastings, W. K. Monte Carlo sampling methods using Markov chains and their applications. *Biometrika*, 57(1):97–109, 04 1970. ISSN 0006-3444.
- Hohenberg, P. C. and Halperin, B. I. Theory of dynamic critical phenomena. *Reviews of Modern Physics*, 49(3): 435, 1977.
- Iserles, A. *A first course in the numerical analysis of differential equations*. Number 44. Cambridge university press, 2009.
- Jordan, M. I., Ghahramani, Z., Jaakkola, T. S., and Saul, L. K. An introduction to variational methods for graphical models. *Machine learning*, 37(2):183–233, 1999.

- Jordan, R., Kinderlehrer, D., and Otto, F. The variational formulation of the fokker–planck equation. *SIAM journal on mathematical analysis*, 29(1):1–17, 1998.
- Kingma, D. P., Salimans, T., Jozefowicz, R., Chen, X., Sutskever, I., and Welling, M. Improved variational inference with inverse autoregressive flow. In *Advances in neural information processing systems*, pp. 4743–4751, 2016.
- Lacombe, G. and Mas-Gallic, S. Presentation and analysis of a diffusion-velocity method. In *ESAIM: Proceedings*, volume 7, pp. 225–233. EDP Sciences, 1999.
- Li, L., Liu, J.-G., Liu, Z., and Lu, J. A stochastic version of stein variational gradient descent for efficient sampling. *arXiv preprint arXiv:1902.03394*, 2019.
- Liu, C. An introduction of elastic complex fluids: an energetic variational approach. In *Multi-Scale Phenomena in Complex Fluids: Modeling, Analysis and Numerical Simulation*, pp. 286–337. World Scientific, 2009.
- Liu, C. and Wang, Y. On lagrangian schemes for the multidimensional porous medium equations by a discrete energetic variational approach. *arXiv preprint arXiv:1905.12225*, 2019.
- Liu, C. and Wang, Y. A variational lagrangian scheme for a phase field model: A discrete energetic variational approach. *arXiv preprint arXiv:2003.10413*, 2020.
- Liu, C. and Zhu, J. Riemannian stein variational gradient descent for bayesian inference. In *Thirty-Second AAAI Conference on Artificial Intelligence*, 2018.
- Liu, C., Zhuo, J., Cheng, P., Zhang, R., and Zhu, J. Understanding and accelerating particle-based variational inference. In *International Conference on Machine Learning*, pp. 4082–4092, 2019.
- Liu, Q. Stein variational gradient descent as gradient flow. In *Advances in neural information processing systems*, pp. 3115–3123, 2017.
- Liu, Q. and Wang, D. Stein variational gradient descent: A general purpose bayesian inference algorithm. In *Advances in neural information processing systems*, pp. 2378–2386, 2016.
- Lu, J., Lu, Y., and Nolen, J. Scaling limit of the stein variational gradient descent: The mean field regime. *SIAM Journal on Mathematical Analysis*, 51(2):648–671, 2019.
- Matthes, D. and Plazotta, S. A variational formulation of the bdf2 method for metric gradient flows. *ESAIM: Mathematical Modelling and Numerical Analysis*, 53(1): 145–172, 2019.
- Metropolis, N., Rosenbluth, A. W., Rosenbluth, M. N., Teller, A. H., and Teller, E. Equation of state calculations by fast computing machines. *The journal of chemical physics*, 21(6):1087–1092, 1953.
- Mika, S., Ratsch, G., Weston, J., Scholkopf, B., and Mullers, K.-R. Fisher discriminant analysis with kernels. In *Neural networks for signal processing IX: Proceedings of the 1999 IEEE signal processing society workshop (cat. no. 98th8468)*, pp. 41–48. Ieee, 1999.
- Murphy, K. P. *Machine learning: a probabilistic perspective*. MIT press, 2012.
- Neal, R. M. and Hinton, G. E. A view of the em algorithm that justifies incremental, sparse, and other variants. In *Learning in graphical models*, pp. 355–368. Springer, 1998.
- Onsager, L. Reciprocal relations in irreversible processes. i. *Physical review*, 37(4):405, 1931a.
- Onsager, L. Reciprocal relations in irreversible processes. ii. *Physical review*, 38(12):2265, 1931b.
- Osher, S., Wang, B., Yin, P., Luo, X., Barekat, F., Pham, M., and Lin, A. Laplacian smoothing gradient descent. *arXiv preprint arXiv:1806.06317*, 2018.
- Rayleigh, L. Note on the numerical calculation of the roots of fluctuating functions. *Proceedings of the London Mathematical Society*, 1(1):119–124, 1873.
- Rezende, D. J. and Mohamed, S. Variational inference with normalizing flows. *arXiv preprint arXiv:1505.05770*, 2015.
- Salman, H., Yadollahpour, P., Fletcher, T., and Batmanghelich, K. Deep diffeomorphic normalizing flows. *arXiv preprint arXiv:1810.03256*, 2018.
- Santambrogio, F. {Euclidean, metric, and Wasserstein} gradient flows: an overview. *Bulletin of Mathematical Sciences*, 7(1):87–154, 2017.
- Sonoda, S. and Murata, N. Transport analysis of infinitely deep neural network. *The Journal of Machine Learning Research*, 20(1):31–82, 2019.
- Stuart, A. M. Inverse problems: a bayesian perspective. *Acta numerica*, 19:451–559, 2010.
- Tabak, E. G., Vanden-Eijnden, E., et al. Density estimation by dual ascent of the log-likelihood. *Communications in Mathematical Sciences*, 8(1):217–233, 2010.
- Wainwright, M. J., Jordan, M. I., et al. Graphical models, exponential families, and variational inference. *Foundations and Trends® in Machine Learning*, 1(1–2):1–305, 2008.

Wang, D., Tang, Z., Bajaj, C., and Liu, Q. Stein variational gradient descent with matrix-valued kernels. In *Advances in neural information processing systems*, pp. 7834–7844, 2019.

Welling, M. and Teh, Y. W. Bayesian learning via stochastic gradient langevin dynamics. In *Proceedings of the 28th international conference on machine learning (ICML-11)*, pp. 681–688, 2011.